

# The response of wildfire regimes to Last Glacial Maximum carbon dioxide and climate

Olivia Haas<sup>1,2</sup>, Iain Colin Prentice<sup>1,2</sup>, Sandy P. Harrison<sup>1,3</sup>

<sup>1</sup>Leverhulme Centre for Wildfires, Environment and Society, Imperial College London, South Kensington, London SW7 2BW, UK

<sup>2</sup>Georgina Mace Centre for the Living Planet, Department of Life Sciences, Imperial College London, Silwood Park Campus, Buckhurst Road, Ascot SL5 7PY, UK

<sup>3</sup>Geography & Environmental Science, University of Reading, Whiteknights, Reading RG6 6AH, UK

*Correspondence to:* Olivia Haas (o.haas20@imperial.ac.uk)

## Abstract

Climate and fuel availability jointly control the incidence of wildfires. The effects of atmospheric CO<sub>2</sub> on plant growth influence fuel availability independently of climate; but the relative importance of each in driving large-scale changes in wildfire regimes cannot easily be quantified from observations alone. Here, we use previously developed empirical models to simulate the global spatial pattern of burnt area, fire size and fire intensity for modern and Last Glacial Maximum (LGM; ~ 21,000 ka) conditions using both realistic changes in climate and CO<sub>2</sub> and sensitivity experiments to separate their effects. Three different LGM scenarios are used to represent the range of modelled LGM climates. We show large, modelled reductions in burnt area at the LGM compared to the recent period, consistent with the sedimentary charcoal record. This reduction was predominantly driven by the effect of low CO<sub>2</sub> on vegetation productivity. The amplitude of the reduction under low CO<sub>2</sub> conditions was similar regardless of the LGM climate scenario and was not observed in any LGM scenario when only climate effects were considered, with one LGM climate scenario showing increased burning under these conditions. Fire intensity showed a similar sensitivity to CO<sub>2</sub> across different climates but was also sensitive to changes in vapour pressure deficit (VPD). Modelled fire size was reduced under LGM CO<sub>2</sub> in many regions but increased under LGM climates because of changes in wind strength, dryness (DD) and diurnal temperature range (DTR). This increase was offset under the coldest LGM climate in the northern latitudes because of a large reduction in VPD. These results emphasise the fact that the relative magnitudes of changes in different climate variables influence the wildfire regime and that different aspects of climate change can have opposing effects. The importance of CO<sub>2</sub> effects imply that future projections of wildfire must take rising CO<sub>2</sub> into account.

## 1. Introduction

Climate influences the occurrence of wildfires both through fire weather, which affects the probability of wildfire start and spread, and the long-term establishment of vegetation which is strongly controlled by temperature and precipitation (Bradstock, 2010; Pausas & Ribeiro, 2013). It has been suggested that current climate change, driven by increasing atmospheric CO<sub>2</sub> levels, will increase wildfire risk in many regions through increased fuel dryness whilst potentially reducing wildfire risk in some regions due to decreasing fuel availability (e.g. Abatzoglou et al., 2019a; Bowman et al., 2020; Harrison et al., 2021; Rogers et al., 2020). However,

36 atmospheric CO<sub>2</sub> levels also affect fuel loads independently of climate through physiological effects on  
37 photosynthesis which cascade into plant growth rates (Bond et al., 2003; Bond & Midgley, 2012; Kgope et al.,  
38 2010). Much emphasis has been placed on recent and future changes in fire weather (see e.g. Abatzoglou et al.,  
39 2019; Betts et al., 2015; Flannigan et al., 2013; Jolly et al., 2015). However, increases in atmospheric CO<sub>2</sub>  
40 concentrations promote vegetation productivity, thus altering fuel availability and loads, as well as affecting fuel  
41 types through e.g. woody thickening (Buitenwerf et al., 2012; Donohue et al., 2013; Knorr et al., 2016; Martin  
42 Calvo et al., 2014; Martin Calvo & Prentice, 2015; Pausas, 2015). Fuel properties have different effects on  
43 different aspects of the fire regime, with fire size strongly constrained by fuel continuity and fire intensity limited  
44 by fuel loads (Archibald et al., 2013; Haas et al., 2022). Thus, CO<sub>2</sub>-induced changes in vegetation properties will  
45 most likely affect these aspects of wildfire regimes differently.

46 One reason the impact of CO<sub>2</sub> on wildfires is poorly constrained is the difficulty of isolating it based on  
47 observations alone. Satellite records only span ~25 years, a relatively short period to monitor the effect of changing  
48 CO<sub>2</sub> levels on the vegetation properties that influence wildfires. Furthermore, changes in atmospheric CO<sub>2</sub> levels  
49 and climate are temporally correlated, and since both affect vegetation, it difficult to attribute changes in  
50 observations to one or the other. An alternative approach is to use process-based fire-enabled vegetation models  
51 which explicitly account for the physiological effects of CO<sub>2</sub> and can be used to examine the temporal and spatial  
52 patterns of wildfires under different conditions. Process-based models have been used to examine the impact of  
53 climate and atmospheric CO<sub>2</sub> changes on both vegetation and wildfire at the last glacial maximum (LGM; 21,000  
54 years ago) (Martin Calvo et al., 2014; Martin Calvo & Prentice, 2015). The LGM is a useful out-of-sample  
55 experiment since the climate forcing is of similar magnitude as the change expected by the end of the century in  
56 high-end scenarios, though of opposite sign (Kageyama et al., 2021). The LGM had a generally colder and drier  
57 climate than today, with CO<sub>2</sub> levels ~ 185 ppm. Palaeorecords show reduced vegetation productivity and forest  
58 cover (Harrison & Prentice, 2003; Kaplan et al., 2016; Moreno et al., 2018), and ice core and sedimentary charcoal  
59 records indicate reduced biomass burning globally (Albani et al., 2018; Harrison et al., 2022; Marlon et al., 2016;  
60 Rubino et al., 2016). Although this reduction could reflect the colder and drier conditions, model experiments  
61 suggests that low CO<sub>2</sub> also played a crucial role. Experiments using the coupled biogeography and  
62 biogeochemistry model BIOME4 (Kaplan et al., 2003) showed that it was necessary to include the direct effect  
63 of CO<sub>2</sub> to simulate observed global and regional reduction in forest cover during the glacial (Bragg et al., 2013;  
64 Harrison & Prentice, 2003). Similarly, Martin Calvo et al. (2015) showed that low CO<sub>2</sub> was necessary to simulate  
65 the observed reduction of biomass burning in LGM experiments using the LPX fire-enabled vegetation model.

66 In this analysis, we use three empirical models (Haas et al., 2022) to explore the relative importance of  
67 climate and of CO<sub>2</sub> on the global spatial patterns of burnt area, fire size and fire intensity. We performed two  
68 experiments under realistic modern CO<sub>2</sub> and climate conditions (MOD climate/MOD CO<sub>2</sub> and LGM  
69 climate/LGM CO<sub>2</sub>). We also performed two counterfactual sensitivity experiments to quantify the sensitivity of  
70 each wildfire property to climate and CO<sub>2</sub> independently (MOD climate/LGM CO<sub>2</sub> and LGM climate/MOD CO<sub>2</sub>).  
71 Comparisons to LGM charcoal records from the Reading Palaeofire Database (RPD) (Harrison et al., 2022) were  
72 used to examine which experiments provided the most realistic spatial patterns.

## 2. Methods

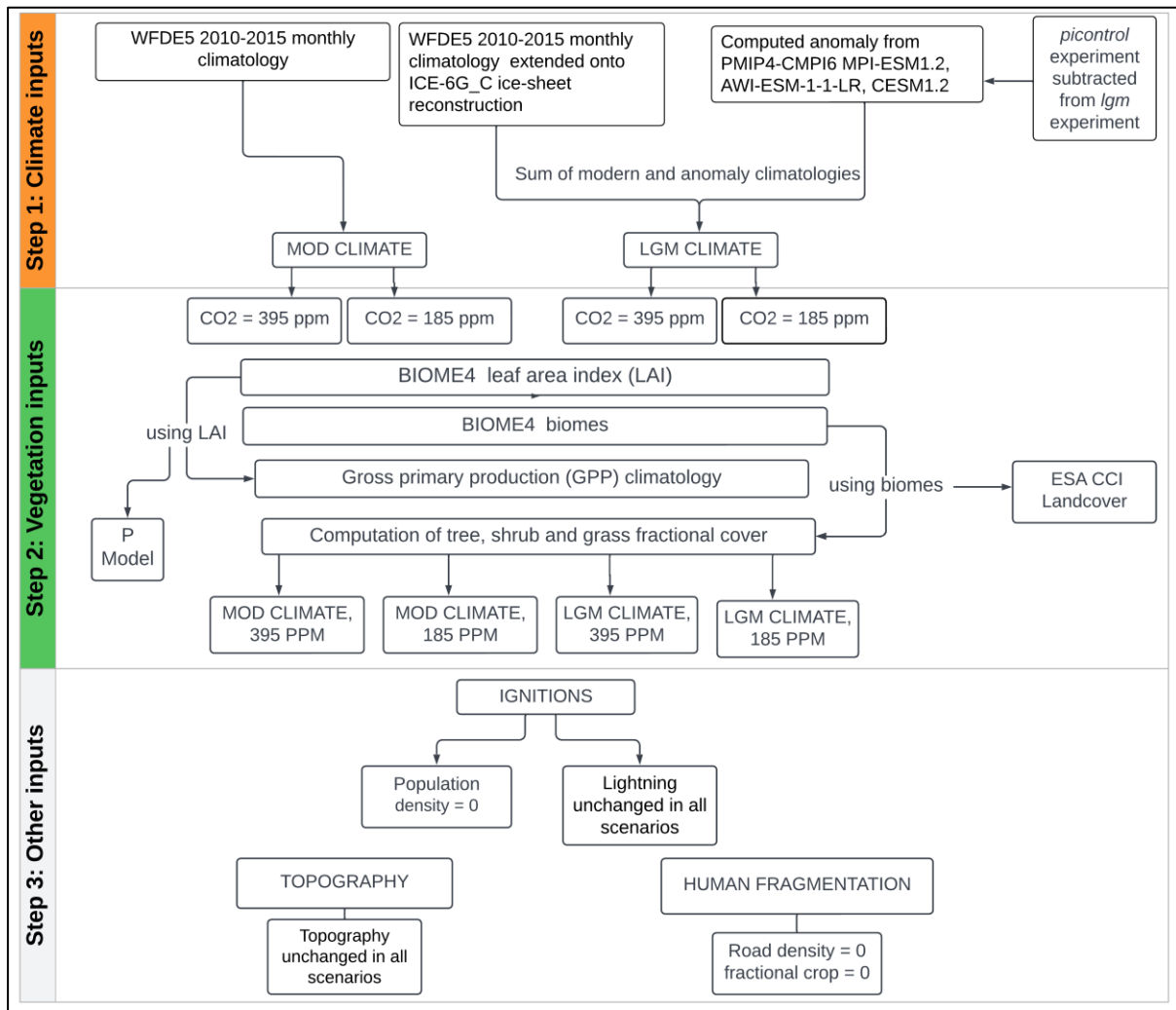


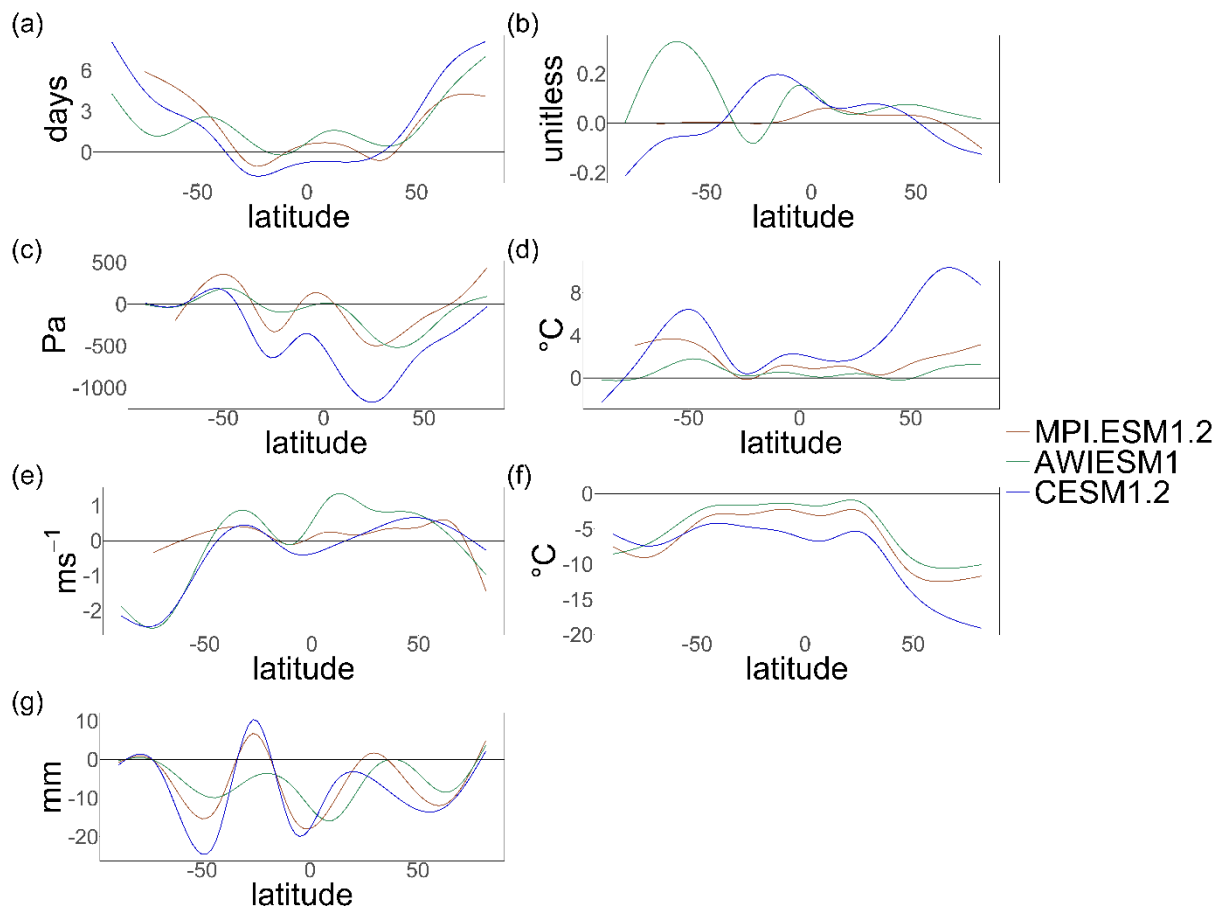
**Figure 1.** Flowchart of the method to obtain each of the four scenarios: MOD climate and MOD CO<sub>2</sub>, LGM climate and LGM CO<sub>2</sub>, MOD climate and LGM CO<sub>2</sub> and LGM climate and LGM CO<sub>2</sub>.

Haas et al (2022) developed empirical models of the global spatial patterns of burnt area (BA), fire size (FS) and fire intensity (FI) using generalised linear modelling (GLM) of modern observations. Here we use these models to simulate the global spatial patterns of burnt area (BA), fire size (FS) and fire intensity (FI) under four climate/ CO<sub>2</sub> scenarios (Figure 1). We used two realistic scenarios: (a) MOD climate and CO<sub>2</sub> conditions and (b) LGM climate and CO<sub>2</sub>. We ran two sensitivity experiments (a) combining MOD climate and LGM CO<sub>2</sub> and (b) combining LGM climate and MOD CO<sub>2</sub> levels. The empirical models use climate, vegetation, topography, lightning ignitions, land cover, road density and human population density as predictors to represent the environmental controls on each of the wildfire properties.

Modern (MOD) climate data (daily temperature (T), daily precipitation (P), photosynthetic photon flux density (PPFD), monthly wind speeds (wind), vapour pressure deficit (VPD), monthly specific humidity (huss), cloud cover (cld), monthly pressure (Pa)) were obtained from the WFDE5 bias-adjusted ERA5 database (Cucchi et al., 2020) for 2010 to 2015. The number of monthly dry days (DD) (days with  $\leq 1$ mm of precipitation), monthly diurnal temperature range (DTR) (daily maximum temperature – daily minimum temperature) and monthly

91 vapour pressure deficit (VPD), a function of specific humidity, temperature and pressure were all calculated  
 92 following the methodology in Haas et al. (2022). Seasonal climatologies were derived for all variables eliminating  
 93 inter-annual variability. For each grid cell, values from the month with (on average) the maximum number of DD,  
 94 the largest DTR, and the highest VPD were selected. Wind speed value was taken from the hottest month of the  
 95 year (determined from the WFDE5 2 m air temperature (Cucchi et al., 2020)). For lightning, the mean value over  
 96 the seasonal climatology was selected. A seasonality predictor to account for wet vs dry seasons was constructed  
 97 by dividing the range of monthly values from the seasonal DD climatology by the mean value of all 12 months.  
 98 Expanded ice sheets in North America, Fennoscandia, Greenland, and Antarctica resulted in global sea levels ~  
 99 120 m lower than today at the LGM. The modern climate data were extrapolated out onto the exposed shelves  
 100 using the ICE-6G\_C (Peltier et al., 2015) boundary conditions and a nearest neighbour approach from the  
 101 *GeoInterpolation* package in R.

102



103

104

105 **Figure 2.** Latitudinal distribution of the LGM-MOD climate anomalies for MPI.ESM1.2 (orange), AWI-  
 106 ESM1.2 (pink) and CESM1.2 (brown) for (a) the maximum number of dry days, (b) the seasonality of dry days,  
 107 (c) maximum monthly VPD, (d) maximum monthly DTR, (e) maximum monthly mean wind speeds, (f) mean  
 108 monthly temperature and (g) mean monthly total precipitation. The zero-intercept line represents no change  
 109 between LGM and MOD climate, with negative values representing lower values at the LGM and positive  
 110 values representing higher values at the LGM.

111

112 LGM climate data were obtained from three models participating in the Palaeoclimate Modelling  
 113 Intercomparison Project (PMIP) contribution to the sixth phase of the Coupled Model Intercomparison Project  
 114 (CMIP6), AWI-ESM-1-1-LR (short name: AWIESM1) (Lohmann et al., 2020; Sidorenko et al., 2015),  
 115 MPI\_ESM1.2 (Mauritsen et al., 2019), CESM1.2 (F. Li et al., 2013; Tierney et al., 2020) to represent a range of  
 116 LGM climates (Figure 2). A seasonal climatology was derived for each climate variable from the PMIP *picontrol*  
 117 experiment (pre-industrial conditions, PI) and the PMIP *lgm* experiment of the PMIP4-CMIP6 simulations. The  
 118 difference between the PI and LGM values (LGM-PI climate anomalies) were calculated and added to the MOD  
 119 climatology (LGM-MOD climate anomalies) (see Figure 1). We use the term climate anomalies to refer to the  
 120 difference between the MOD climatology for each climate variable and the computed bias-adjusted LGM  
 121 climatology for the same variable, consistent with the PMIP4 protocol (Kageyama et al., 2017). The use of  
 122 anomalies is designed to minimise the impact of systematic model biases on the derived climate. This approach  
 123 provided three LGM climate scenarios, resulting in twelve experiments for BA, FS and FI respectively.

124 We obtained MOD and LGM vegetation and gross primary production (GPP) using the coupled  
 125 biogeography and biogeochemistry model BIOME4 (Kaplan et al., 2003) and a simple optimality-based model of  
 126 GPP, the P Model (Wang et al., 2017; Stocker et al., 2020). BIOME4 was used to simulate biome distribution  
 127 with modern day climate data (T, P, cld) setting CO<sub>2</sub> levels to 395 ppm (the annual mean from 2010-2015) and  
 128 185 ppm in turn. LGM biome distributions were simulated using the three different LGM scenarios, again setting  
 129 CO<sub>2</sub> levels to 395 ppm and 185 ppm respectively. We derived mean fractional tree, shrub, and grass cover for  
 130 each of these twelve experiments using the mean values for each biome from ESA CCI Landcover (W. Li et al.,  
 131 2018). We also calculated fAPAR for each experiment from the leaf area index (LAI) computed by BIOME4 and  
 132 obtained fractional cover of C<sub>4</sub> plants (see S1). We computed global monthly C<sub>3</sub> and C<sub>4</sub> photosynthesis using the  
 133 P model using appropriate combinations of climate (T, VPD, ppfd and Pa), BIOME4-derived fAPAR and CO<sub>2</sub>  
 134 concentration for the MOD and LGM scenarios (see Figure 1). Total GPP was calculated as:

$$135 \quad GPP_{monthly} = GPP_{C3}(1 - C4_{fraction}) + GPP_{C4}C4_{fraction} , \quad (1)$$

136 with  $GPP_{C3}$  and  $GPP_{C4}$  representing monthly C<sub>3</sub> and C<sub>4</sub> GPP values from the P Model and  $C4_{fraction}$  representing  
 137 the fractional C<sub>4</sub> cover from BIOME4 (see Table1).

138

Scenario	Modern climate	MPI_ESM1.2	AWIESM1	CESM1.2 LGM
Modern CO <sub>2</sub> (395 ppm)	149.37	106.63	112.06	88.44
LGM CO <sub>2</sub> (185 ppm)	66.54	55.49	69.61	50.37

139

140 **Table 1.** Total annual gross primary production (GPP) (in PgC) estimates for each scenario.

141

142 This approach led to estimates of total BA, median FS, and median FI under modern conditions of a  
 143 similar magnitude to the original GLM models and other global estimates (Andela et al., 2019; Humber et al.,  
 144 2019) (Table 2).

145 Topographic and lightning variables were assumed not to change between the LGM and the present day.  
 146 We used modern values, extrapolated out onto the exposed shelves, for the LGM experiments. The GLMs (Haas  
 147 et al., 2022) include predictors associated with human activity, specifically human population density, road density  
 148 and cropland cover. Population density is used as a measure of potential human ignitions and road density and

149 cropland cover as measures of landscape fragmentation. Including these anthropogenic predictors in the GLM  
150 models was found to be essential to capture the global drivers of the observed spatial patterns of wildfires (Haas  
151 et al., 2022). This is because modern fire regimes are influenced by human activity at a global scale (e.g. Marlon  
152 et al., 2008; Bowman et al., 2020; Harrison et al., 2021). However, although the practice of foraging for plants by  
153 some hunter-gatherer communities at the LGM has been shown (Liu et al., 2013), we presume that there was no  
154 large-scale agriculture (or road networks) at the LGM. Additionally, information about pre-agricultural population  
155 sizes is limited and highly uncertain (see e.g. Williams et al., 2013; Gautney & Holliday, 2015) and though some  
156 regional models of human population do exist (Tallavaara et al., 2015), a reliable global product is not yet  
157 available. To avoid confounding effects due to the high uncertainty of human impacts on global wildfire regimes,  
158 we decided to exclude these anthropogenic predictors in all the experiments by setting them to zero. This ensured  
159 that differences between the experiments were driven solely by climate and CO<sub>2</sub>. We performed sensitivity  
160 analysis to examine the impact of setting human predictors to zero under modern and LGM conditions (see S2).  
161 Whilst BA and FS increase in the modern sensitivity analyses (especially in areas with high road density and  
162 cropland density such as Europe and India) the effect was negligible for FI, highlighting the sensitivity of BA and  
163 FS to human activity. Under LGM conditions, the effect of including human population was negligible for all  
164 three fire properties. This reflects the slight and localised human impact on the natural landscape at the LGM  
165 (Black et al., 2007; Fuller et al., 2014; Portenga et al., 2016).

166

167 When modelled GPP values were 0, BA, FS and FI was automatically set to 0. Modelled BA values smaller  
168 than 0.001 were assumed to imply no burning, thus under these conditions FS and FI were also assumed to be 0  
169 since both GLM models were trained on data of existing fires (see S3).

170 The resulting BA, FS and FI anomalies refer to the difference between the MOD climate/MOD CO<sub>2</sub>  
171 experiment and the three other experiments since each experiment is considered to represent the long-term average  
172 spatial pattern for each fire property under the set experimental conditions. We used the sensitivity experiments  
173 to quantify the separate effects of CO<sub>2</sub> and climate on BA, FS and FI independently. We then used the realistic  
174 experiments to identify which predictors were driving the largest change between MOD and the three LGM  
175 scenarios by excluding one predictor at a time from the GLM models, re-running the LGM experiments and  
176 identifying which excluded variable caused the greatest change in the BA, FS and FI MOD-LGM anomalies in  
177 each grid-cell. Comparing these results to the BA, FS and FI MOD-LGM anomalies of the full GLM models  
178 allowed us to determine if the predictor was responsible for an increase or a decrease in BA, FS and FI.

179 We also compared the spatial patterns of BA, FS and FI with sedimentary charcoal data from the Reading  
180 Palaeofire Database (RPD; Harrison et al., 2022). Sedimentary charcoal records provide a record of fire activity  
181 but may reflect changes in both burnt area or completeness of combustion (Power et al., 2008) so this comparison  
182 allowed us firstly to establish which of the fire regimes properties was most closely reflected in these records and  
183 secondly which of the scenarios produced the most realistic patterns of burning. Model outputs and the charcoal  
184 records were re-gridded to the coarsest resolution of the three climate models (2.5° x 1.875° resolution). We  
185 calculated the number of correctly predicted BA, FS or FI anomalies (same sign within a given grid-cell),  
186 separating positive and negative BA, FS or FI anomalies to assess the rate of false positives as well as false  
187 negatives for each scenario and each LGM climate scenario.

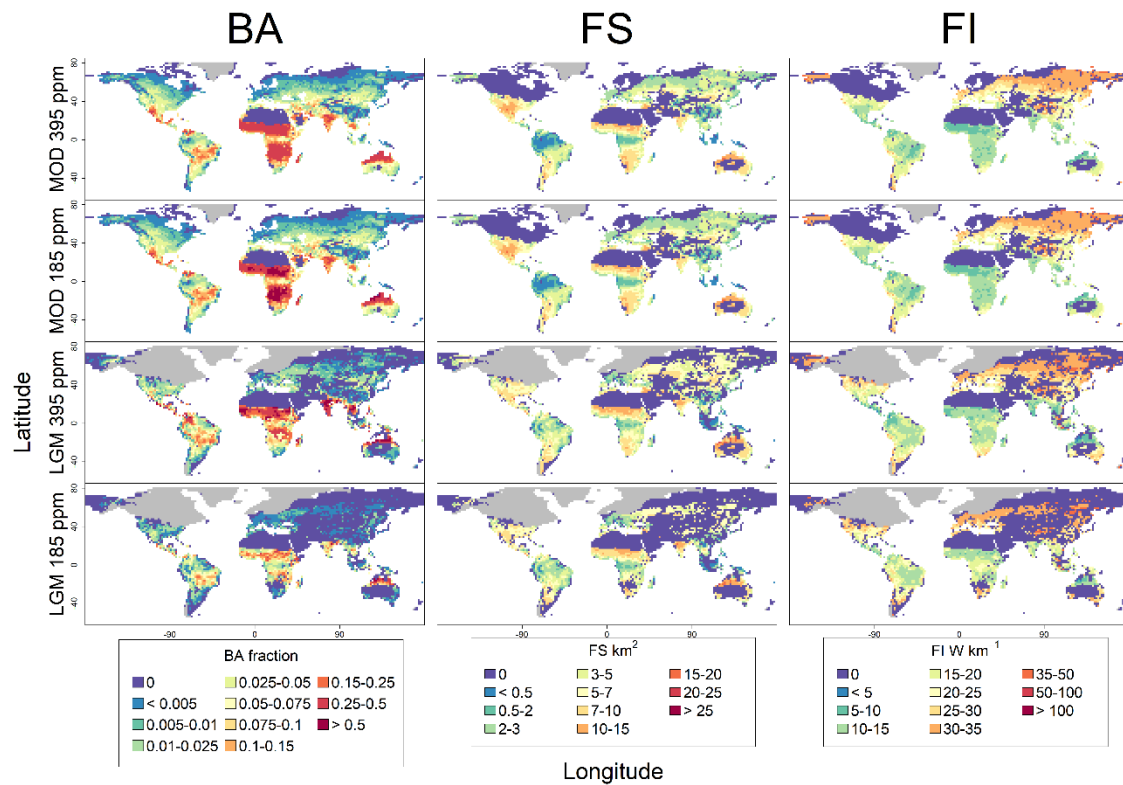
188 **3. Results**

189 Global BA was substantially reduced compared to the realistic MOD scenario under all three realistic  
190 LGM scenarios, decreasing by 72% for the coldest CESM1.2 LGM scenario, 62% for the MPI-ESM1.2 LGM  
191 scenario and 41% for the warmest AWIESM1 LGM scenario. The largest decreases were observed in sub-Saharan  
192 Africa (excluding the tropical regions) as well as northern Australia and the Indian subcontinent (MPI-ESM1.2  
193 and CESM1.2 LGM scenarios). Some increases in BA were observed in Alaska (MPI-ESM1.2 and AWIESM1  
194 LGM scenarios) as well as south-East Asia, Indonesia, Papua-New-Guinea, and the northern tip of Australia.  
195 Increases in Somalia and Central America were also observed (MPI-ESM1.2 and AWIESM1 LGM scenarios).  
196 The number of grid cells (excluding ice covered cells) in which no burning occurred was 3 times higher in the  
197 MPI-ESM1.2 and AWIESM1 LGM scenarios and 4 times higher in the CESM1.2 LGM scenario compared to the  
198 realistic MOD scenario. This was driven by the expansion of desert and tundra biomes at the LGM. The Arabian  
199 plate, Middle East, inland China and Australia, and the tips of South America and Africa saw burning reduced to  
200 zero. Nearly all burning above 60°N was excluded, except for Alaska under the MPI-ESM1.2 and AWIESM1  
201 LGM scenarios, with the exclusion extending down to 50°N for the CESM1.2 LGM scenario (see S3).

202 Globally, there was a large decrease in global median FS and FI when considering all grid-cells (not  
203 covered in ice) because of overall global reduction in burning. Under all three LGM scenarios, global median FS  
204 and FI were reduced to 0 compared to ~5km<sup>2</sup> for FS and 40W.km<sup>2</sup> for FI. However, when excluding grid-cells in  
205 which no burning occurred, both global median FS increased compared to the realistic MOD scenario (by ~16%  
206 under the two less conservative scenarios (MPI-ESM1.2 and AWIESM1) and by 12% under the CESM1.2 LGM  
207 scenario). The main increases in FS occurred in the Central America, Amazonia, tropical Africa as well as the  
208 Indian Subcontinent and Europe and Asia between 30°N and 60°N (except for CESM1.2 which had very few  
209 positive FS anomalies). The largest reductions were observed North America, southern Australia, Middle East,  
210 and the rest of Eurasia. Global median FI also increased in regions that were burning under two of the LGM  
211 scenarios, by 11% under the CESM1.2 LGM scenario and by 4% for MPI.ESM1.2 LGM scenario. Under the  
212 AWIESM1 LGM scenario global median FI decreased by 2% even when excluding grid-cells that were not  
213 burning. Despite this, changes in FI were spatially consistent across all three LGM scenarios, with increases in FI  
214 occurring primarily across the American and African continents, as well as the Mediterranean Basin and Europe  
215 and decreases occurring in Asia and inland Australia.

216

217



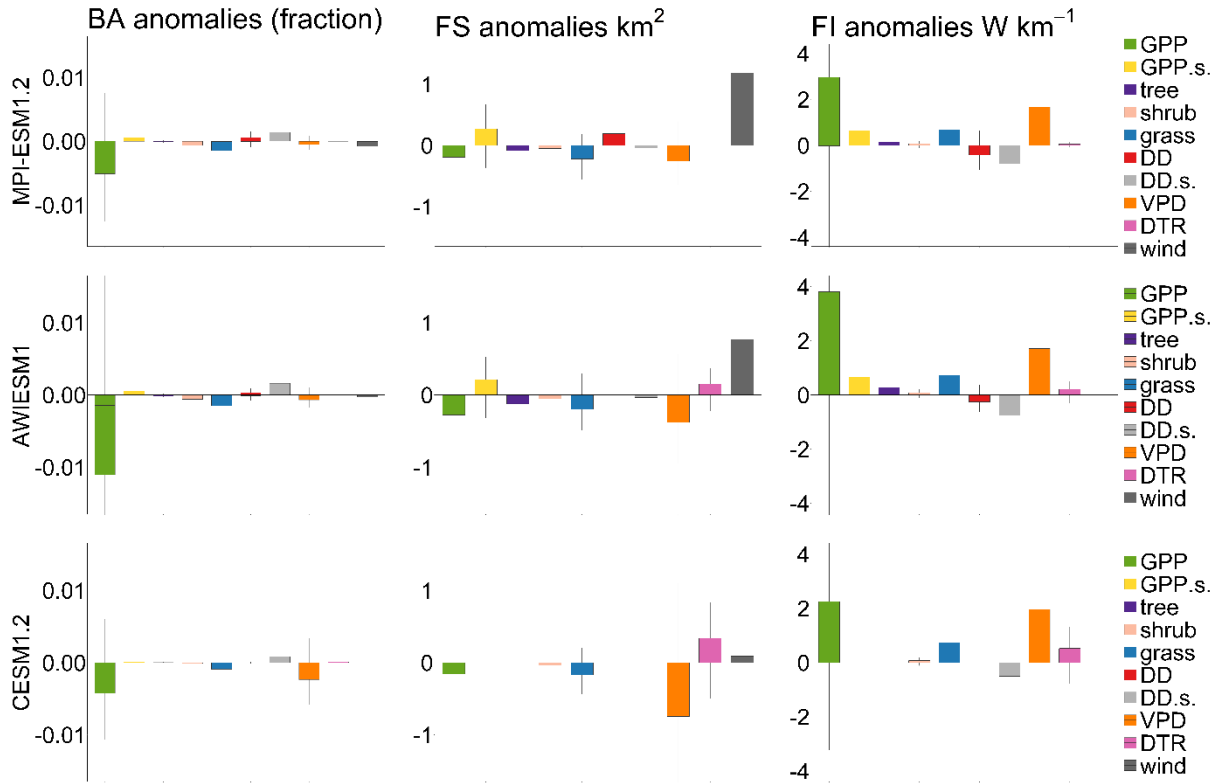
218  
 219 **Figure 3.** Experiments for BA, FS and FI for MPI-ESM1.2 LGM scenario (MOD 395 ppm and LGM 185 ppm  
 220 represent the realistic modern-day simulation and LGM simulation, whilst MOD 185 ppm and LGM 395 ppm  
 221 represent the CO<sub>2</sub> and climate sensitivity experiments respectively. The ice is shown in grey). (The other  
 222 experiments can be found in S3)  
 223

224 Under low CO<sub>2</sub> levels with MOD climate (MOD climate/LGM CO<sub>2</sub>) global BA decreased by ~ 70%  
 225 under all three LGM scenarios (72% for CESM1.2 and AWIESM1, 73% for MPI-ESM1.2). Despite larger global  
 226 decreased BA compared to the realistic LGM scenarios, the number of grid cells in which no burning occurred  
 227 was only 1.7 times higher for MPI-ESM1.2 and AWIESM1 LGM scenarios and 1.5 times CESM1.2 LGM  
 228 scenario compared to the realistic MOD scenario. The spatial pattern was consistent across all three LGM  
 229 scenarios, with very few grid-points showing a positive BA anomaly relative to the MOD experiment. Though FS  
 230 increased slightly under this sensitivity experiment when burning did occur, this increase was concentrated in the  
 231 tropical regions of South America and Africa (mainly Amazonia), (except for AWIESM1 were increases were  
 232 observed across Eurasia). In burning grid-cells, global median FI increased by ~ 15-18% in this sensitivity  
 233 experiment (18% for MPI-ESM1.2 and CESM1.2, and 15% for AWIESM1). This spatial pattern was also  
 234 consistent as with BA, with very few negative FI anomalies, except for regions ~ 20-30°N and ~20-30°S.

235 Under MOD CO<sub>2</sub> and LGM climate, BA decreased by 41% compared to the MOD experiment for the  
 236 CESM1.2 LGM scenario and by 4% for the MPI-ESM1.2 LGM scenario but increased by 48% for the AWIESM1  
 237 LGM scenario, showing a strong sensitivity to climate. The number of grid cells in which no burning occurred  
 238 was of similar amplitude to the previous sensitivity experiment for the MPI-ESM1.2 and AWIESM1 LGM  
 239 scenarios (~1.8 times higher compared to the realistic MOD scenario) but was much higher for the CESM1.2  
 240 LGM scenario (~3.5 increase). When burning occurred, the global median FS increased under all LGM scenarios



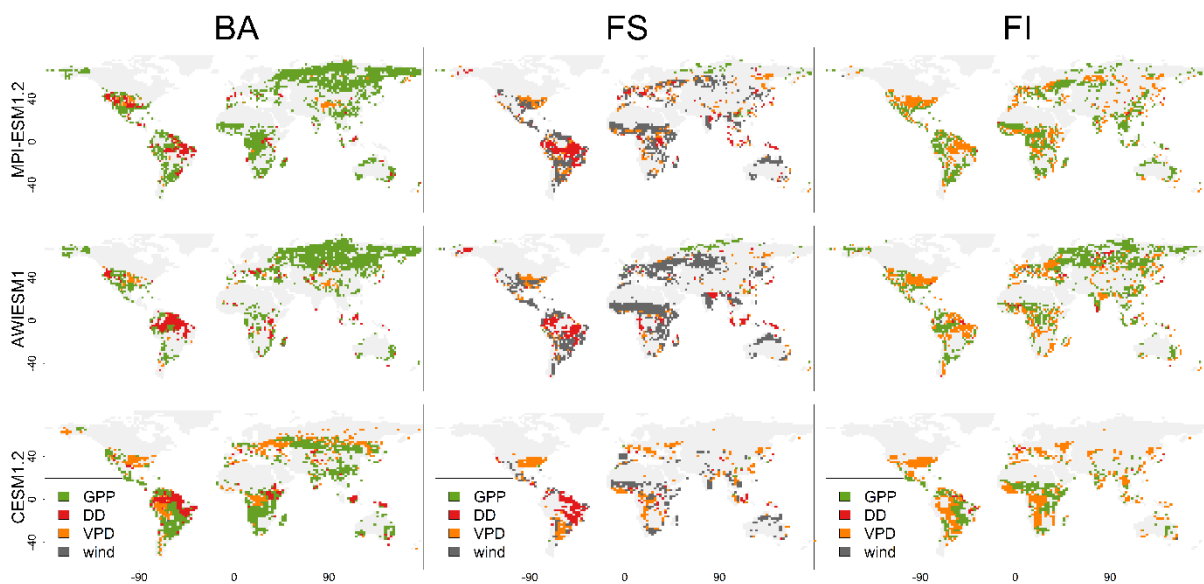
241 by 17% for CESM1.2, 25% for MPI-ESM1.2 and 23% for AWIESM1. These increases were concentrated in  
 242 tropical Africa, central America, and Russia, with decreases shown in North America and South Africa. Global  
 243 median FI also increased under this sensitivity experiment by 2-3% for AWIESM1 and MPI-ESM1.2 but  
 244 decreased by 5% for CESM1.2 LGM scenario, with decreases concentrated in Eurasia and North America.  
 245



246  
 247 **Figure 4.** Boxplots showing relative importance of each predictor (GPP: gross primary production,  
 248 GPP.s.: GPP seasonality, tree; tree cover, shrub; shrub cover, grass; grass cover, DD: dry days, DD.s.: dry days  
 249 seasonality, VPD: vapour pressure deficit, DTR: diurnal temperature range, wind: wind speed) in driving the  
 250 BA, FS or FI anomaly between the MOD 395 ppm and LGM 185 ppm experiment. For each grid cell common  
 251 to both experiments (on modern-day continental shelves and masking the LGM ice sheets), the predictor which  
 252 caused the largest change in the anomaly between the two experiments when it was excluded from the GLM  
 253 model was retained, it is the change in anomaly that is shown here. This was taken as an indicator of relative  
 254 importance of that predictor in driving the observed change for (a) the AWIESM1 LGM scenario, (b) the MPI-  
 255 ESM-1.2 LGM scenario and (c) the CESM1.2 LGM scenario. A positive anomaly indicates the variable caused  
 256 an increase in BA, FS or FI at the LGM and a negative anomaly indicates the variable caused a decrease in BA,  
 257 FS or FI at the LGM.  
 258

259 Reductions in BA between the MOD and LGM scenarios were driven primarily by changes in GPP, grass  
 260 cover, VPD and to a lesser extent dryness (dry days (DD) and dry-day seasonality (DD.s)). Changes in FI were  
 261 driven by changes in GPP as well as VPD, with changes in GPP seasonality also leading to increased FI in inland  
 262 regions, reflecting both changes in climate and CO<sub>2</sub> levels for BA and FI. Increased FS was largely driven by  
 263 increased wind speeds, as well as DD and diurnal temperature range (DTR) reflecting a strong climate effect as

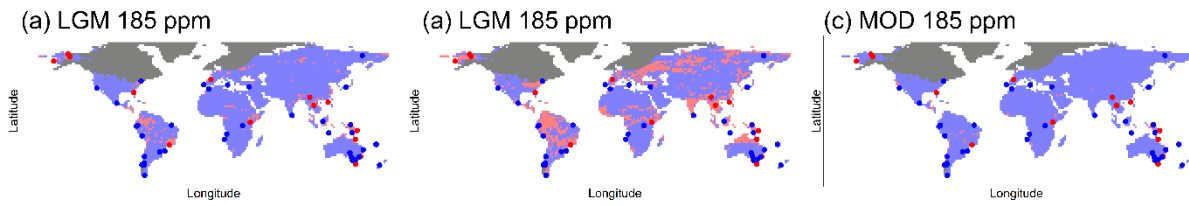
264 well as GPP seasonality. Decreases in FS driven were by changes in GPP and grass cover, as well as VPD under  
 265 the CESM1.2 LGM scenario and DTR under the AWIESM1 LGM scenario (Figure 4). Changes in GPP and grass  
 266 cover were responsible for the largest reductions in burning, with these vegetation effects concentrated across  
 267 Africa and much of Eurasia (see Figure 5). In Amazonia, changes in DD were the most important factor, reducing  
 268 BA and FS (except for MPI-ESM1.2 which saw increased FS driven by DD). Increased BA in western Alaska  
 269 was driven by GPP in the MPI-ESM-1.2 and AWIESM1 LGM scenarios. Increased BA in tropical regions were  
 270 driven by grass cover, GPP and DD changes. Changes in VPD across the northern latitudes, especially of north  
 271 America and Europe, led to decreased BA in the most conservative CESM1.2 LGM scenario. FS decreased across  
 272 the Americas and Eurasia in the CESM1.2 LGM scenario because of low VPD values which reduced the  
 273 occurrence of burning and offset the increases caused by wind speed and DTR in the other two LGM scenarios.  
 274 Low values of VPD drove increases in FI across eastern North America, South America, western Africa, and  
 275 South-East Asia.



276  
 277 **Figure 5.** Map showing selection of four variables (GPP in green, DD in red, VPD in orange and wind in grey)  
 278 responsible for some of the most important grid-cell drivers in reducing BA, increasing FS and FI for (a)  
 279 AWIESM1 LGM scenario, (b) MPI-ESM1.2 LGM scenario and (c) CESM1.2 LGM scenario. Maps of most  
 280 important grid-cell drivers for all variables and all experiments can be found in S3.

281  
 282 Comparing the spatial patterns of the simulated BA anomalies with charcoal-based reconstructions of  
 283 the sign of changes in biomass burning (RPD; Harrison et al., 2022) showed that the best overall match occurred  
 284 when both the climate and CO<sub>2</sub> effect were considered, with a success rate of ~ 39-45% depending on the climate  
 285 scenario. The MPI-ESM1.2 and AWIESM1 LGM scenarios produced the best overall matches. None of the MOD  
 286 climate/LGM CO<sub>2</sub> experiments identified any of the positive BA anomalies shown by the charcoal records. The  
 287 LGM climate/MOD CO<sub>2</sub> experiments identified around half (~ 10-17%) of the negative BA anomalies identified  
 288 by the realistic experiment (17-20%) and the MOD climate/LGM CO<sub>2</sub> sensitivity experiment, and only performed  
 289 marginally better than the realistic experiment in identifying the positive BA anomalies (Table 3). Thus, although  
 290 this sensitivity experiment produced a similar overall agreement with the reconstructions as LGM climate/LGM  
 291 CO<sub>2</sub> simulations, only the realistic scenarios produced similar success rates for both the negative and positive BA

292 anomalies. Climate change alone produced too few negative anomalies matches; CO<sub>2</sub> changes alone resulted in  
 293 no positive anomaly matches.



294  
 295  
 296  
 297  
 298  
 299  
 300  
 301

**Figure 6.** Comparison of BA anomalies between the experiment outputs from the MPI-ESM1.2 LGM scenario with charcoal records from the Reading Palaeofire Database (RPD) for (a) the realistic LGM experiment (b) the LGM climate/MOD CO<sub>2</sub> sensitivity experiment and (c) the MOD climate/LGM CO<sub>2</sub> sensitivity experiment. The modelled positive LGM-MOD anomalies are shown in red and LGM-MOD negative anomalies in blue. Dotted red (positive anomaly) and blue (negative anomaly) points show the location of the RPD records for the LGM. The LGM ice sheets are shown in dark blue.

BA experiments		MPI_ESM1.2			AWIESM1			CESM1.2 LGM		
Scenario	RPD	LGM	MOD	LGM	LGM	MOD	LGM	LGM	MOD	LGM
		190	190	395	190	190	395	190	190	395
Negative RPD anomalies										
Number of records	35	20	21	13	17	21	10	20	20	17
Successful identification (percentage)		57	60	37	49	60	29	57	57	49
Positive RPD anomalies										
Number of records	16	3	0	8	6	0	5	0	0	3
Successful identification (percentage)		19	0	50	38	0	31	0	0	19
Total RPD anomalies										
Number of records	51	23	21	21	23	21	15	20	20	20
Successful identification (percentage)		45	41	41	45	41	29	39	39	39

302  
 303  
 304  
 305  
 306  
 307  
 308

**Table 2.** Comparison of sign in BA anomalies (between the MOD climate/MOD CO<sub>2</sub> experiment and other three experiments respectively) at the location of each RPD charcoal-based reconstruction record. A positive anomaly represents increased biomass burning, and a negative anomaly represents decreased biomass burning. A successful identification means that the sign of the experiment anomaly and the sign of the RPD charcoal-based reconstructions are the same.

309 The sign of the charcoal records could reflect changes in FS or FI as well as BA. However, the success rates  
 310 in predicting the sign of the charcoal anomalies (both positive and negative) were not as good for FS (27-31%)  
 311 and FI (24-30%) than those obtained for BA for the realistic LGM experiment. Furthermore, both FS and FI did  
 312 not perform any better than BA under any experiment, with the sensitivity experiments matching the charcoal  
 313 anomalies slightly better for FS and FI than the realistic LGM experiment (see S4).

314 **4. Discussion**

315 Our simulations show a global reduction in burning at the LGM but increased median fire size and  
316 intensity when burning did occur. BA, FS and FI were all sensitive to changes in vegetation driven directly by  
317 CO<sub>2</sub> levels alone. BA and FI were most sensitive to this effect, with the climate effect dampening the effect of  
318 CO<sub>2</sub> alone when both are included. The largest reductions in burning occurred when only the CO<sub>2</sub> effect was  
319 considered although this experiment had fewer regions in which burning was excluded completely. This suggests  
320 that the reduction in burning was more spatially consistent and widespread under these conditions than when both  
321 effects were accounted for. The sensitivity of BA to CO<sub>2</sub> is explained by the reduction in fuel availability under  
322 low CO<sub>2</sub>, a strong constraint on burnt area. For FI, including a CO<sub>2</sub> effect also amplified the overall global signal.  
323 This CO<sub>2</sub> effect is most likely driven by the negative relationship between GPP and FI fitted by the empirical  
324 model. Whilst this relationship might seem counter-intuitive, it has a sound basis. The most intense fires occur in  
325 regions with a seasonal variation in productivity rather than the most productive environments such as tropical  
326 forests (Archibald et al., 2013). High productivity can (under some climate conditions) increase the frequency of  
327 burning, which also reduces fuel loads (Rodrigues et al., 2019). Under appropriate climate conditions, there can  
328 be long-term fuel build-up in areas of low productivity that is not offset by frequent burning. All these factors  
329 help to explain why FI is not reduced at the LGM when burning occurs even though BA is. Low CO<sub>2</sub> decreased  
330 FS except for tropical regions and reduced the impact of climate in the realistic scenarios. We hypothesize this is  
331 because of decreased productivity leading to patchier vegetation, and hence reduced fuel continuity, which is a  
332 factor limiting wildfire spread (Dial et al., 2022; Schertzer et al., 2015).

333 Changes in climate alone also affected all three modelled wildfire properties. The climate effect was  
334 larger than the CO<sub>2</sub> effect across all models for FS, with increases in wind, DD and DTR driving the change. BA  
335 was particularly sensitive to the amplitude of climate change: climate change alone greatly reduced BA under the  
336 coldest LGM scenario (CESM1.2), had a limited effect in the intermediate LGM scenario (MPI-ESM1.2) and  
337 increased BA in the warmest LGM scenario (AWIESM1). The amplitude of change in VPD, a measure of  
338 atmospheric moisture, relative to other climate variables was especially important in influencing overall trends.  
339 In the case of BA, large decreases in VPD under the CESM1.2 climate scenario led to much more substantial  
340 reductions, most likely due to an increase in fuel moisture. Additionally, though stronger winds and increased  
341 DTR were the main drivers of larger wildfires at the LGM, low VPD values in CESM1.2 severely limited FS and  
342 FI in the northern latitudes. VPD has been shown to influence wildfire ignition and wildfire spread (Sedano &  
343 Randerson, 2014), and our results suggest high atmospheric moisture can inhibit fire spread. When vegetation  
344 was sufficiently abundant however, low VPD values were key in driving intensity. Although vegetation  
345 productivity was lower at the LGM, decreased VPD may have contributed to larger fuel build-ups, thus increasing  
346 fuel loads. This highlights the sensitivity of the fire regime not just to overall climate change but the relative  
347 amplitude of change in individual climate variables.

348 Our model results reproduce the global reduction of biomass burning at the LGM observed from ice  
349 cores and sedimentary charcoal records (Daniau et al., 2012; Harrison et al., 2022; Power et al., 2008; Rubino et  
350 al., 2016). Some studies have indicated the occurrence of high-intensity wildfires on the Palaeo-Agulhas Plain of  
351 South Africa, tropical regions, northern Australia, and central China at the LGM (Kraaij et al., 2020; Power et al.,  
352 2008; Rowe et al., 2021; Ruan et al., 2020; M. Song et al., 2023). Our results are consistent with the trends in  
353 these regions. The LGM simulations of BA that account for both climate and CO<sub>2</sub> appear to fit the charcoal records

354 best. The spatial patterns of BA at the LGM were more consistent with the patterns shown by sedimentary charcoal  
355 records than FS and FI, consistent with the assumption that charcoal abundance can be used as a measure of  
356 biomass burning. The FS and FI anomaly patterns were less consistent than that of BA, suggesting a regime of  
357 less burning but larger and more intense wildfires at the LGM could be consistent with the charcoal records.  
358 Whilst FI has been reconstructed from charcoal (e.g. Duffin, 2008; Snitker, 2018) there are currently no  
359 comparable measures that record FS or FI changes globally. Charcoal records are not available from some regions,  
360 further limiting our ability to evaluate the models, particularly in Eurasia and inland South America where low  
361 CO<sub>2</sub> leads to large reductions in BA that are not observed when only climate is considered.

362 Our results are based on simple empirical models for BA, FS and FI. However, the inferred changes in  
363 BA are like those of Martin Calvo et al. (2015) who used the Land surface Processes and eXchanges (LPX)  
364 dynamic global vegetation model. Empirical models have been shown to perform as well as more complex  
365 process-based models in simulating burned area under modern-day conditions (Hantson et al., 2020). Thus, our  
366 conclusions about the relative impact of climate and CO<sub>2</sub> changes on fire properties are unlikely to be adversely  
367 affected by the relative simplicity of the models used. Their simplicity facilitates running multiple scenarios and  
368 diagnosis of the factors influencing changes in wildfire properties.

369 The effect of human activity was not considered in this analysis and as such no conclusions can be drawn  
370 on how human activity may affect these trends. Although this is a limitation, we believe it is unlikely that human  
371 activity would substantially impact the response of wildfire regimes to the changes in climate and CO<sub>2</sub> observed  
372 here. Pre-agricultural hunter-gatherer populations used fire for land management, for example to facilitate hunting  
373 and to promote the local abundance of food plants (Bowman, 1998; Gott, 2005), although recent work indicates  
374 that the burning regimes they practiced tended to reduce fire overall compared to the natural state (see e.g.  
375 Constantine IV et al., 2023). However, the areas suitable for hunter-gatherer populations was much reduced at the  
376 LGM by generally colder and drier climates and hunter-gatherer populations were confined to climatically suitable  
377 refugia (see e.g. Williams et al., 2013; Blinkhorn et al., 2022). Furthermore, although the estimates of population  
378 density are highly uncertain, the LGM population of Australia was less than 5% of the modern population and the  
379 reduction in Africa was even larger (Gautney and Holliday, 2015). Palaeoecological evidence from Australia  
380 suggests that the use of fire by pre-agricultural hunter-gatherers had a low impact on the environment before the  
381 late Holocene (e.g. Black et al., 2007; Fuller et al., 2014; Portenga et al., 2016). Thus, it is unlikely that human  
382 activities during the LGM would have substantially increased fire or offset the impact of the changes in climate  
383 and CO<sub>2</sub> on fire regimes. Previous studies show a weak influence of population and land-use change on driving  
384 global wildfire trends prior to the 18th century (e.g Pechony and Shindell, 2010; Bowman et al., 2020) and a sharp  
385 human-driven decline in wildfire activity since the mid-nineteenth century (e.g Marlon et al., 2008; Wang et al.,  
386 2010). This recent reduction in global biomass burning was most likely driven by population growth and land-use  
387 change leading to increased landscape fragmentation, which tends to suppress fire spread (e.g. Knorr et al., 2014;  
388 Andela et al., 2016; Harrison et al., 2021).

389 These results add to a growing body of literature highlighting the importance of considering not only  
390 changes in wildfire weather but also vegetation properties in projections of future wildfire regimes (e.g. Harrison  
391 et al., 2021; Kuhn-Régner et al., 2021; Pausas & Keeley, 2021). The impact of rising CO<sub>2</sub> levels will most likely  
392 enhance vegetation growth and litter accumulation, which are important controls on fuel availability, continuity,  
393 and load. However, climate and specifically VPD may have opposing effects to that of rising CO<sub>2</sub> levels. Since

394 VPD controls plant growth, increasing VPD can limit ecosystem productivity and tree growth, in turn reducing  
395 fuel loads (Williams et al. 2013). Nevertheless, VPD has also been shown to increase litter fall, thus increasing  
396 available dead fuel (Resco de Dios 2020, De Faria et al. 2017). As such, it is important to consider how temporal  
397 and spatial scales affect the response of vegetation to changing VPD (Grossiord et al., 2020). Although the trade-  
398 offs between future increases in CO<sub>2</sub> and reductions in productivity due to higher temperatures and atmospheric  
399 dryness are not fully understood, this work highlights the importance of considering both. These effects will most  
400 likely not be evenly distributed across the globe (Gonsamo et al., 2021; Piao et al., 2020; van der Sleen et al.,  
401 2015) and CO<sub>2</sub> effects may be more important in some regions than others. In fuel-limited ecosystems, CO<sub>2</sub>  
402 fertilization could increase fuel loads and fuel continuity, increasing overall burnt area but also the potential for  
403 larger and more intense wildfires. This is particularly worrying in regions with anticipated decreases in  
404 atmospheric moisture, especially since evidence suggests rising VPD may only counteract a small proportion of  
405 CO<sub>2</sub>-induced plant growth (Y. Song et al., 2022). Increased woody thickening, for example in tropical South Asia  
406 (Kumar et al., 2021; Scheiter et al., 2020), may also alter fuel loads in regions that are likely to be vulnerable to  
407 ignition under a drier and warmer atmosphere (Clarke et al., 2022). Whilst climate variables such as DD and DTR  
408 have also shown to be strong controls of global wildfires regimes (e.g. Bistinas et al., 2014; Forkel et al., 2019;  
409 Kuhn-Régner et al., 2021), this study highlights the importance of VPD relative to other climate variables in  
410 driving spatial patterns of BA, FS and FI. This is in line with previous studies that have highlighted the important  
411 role of VPD in promoting fuel loads and fire spread (e.g. Diffenbaugh et al., 2021; Grillakis et al., 2022; Duane  
412 et al., 2021; Balch et al., 2022). Correctly projecting changes in fuels in the next century will require considering  
413 both the effect of VPD and effects of CO<sub>2</sub> on plant growth and fuel loads.

414 Our results stress the importance of accounting for the effects of CO<sub>2</sub> on vegetation when considering  
415 how future fire regimes may evolve. Different aspects of the fire regime respond differently to changes in fuel  
416 properties. Without accounting for this crucial effect, our understanding of future risks will remain limited.

417

418 **Code availability.** All code used in this paper is available at freely available for use in RStudio: the code  
419 for the GLM models is available at <https://doi.org/10.6084/m9.figshare.19071044.v1>, and the code to generate the  
420 experiments are available at: <https://doi.org/10.6084/m9.figshare.22285303.v2> and  
421 <https://doi.org/10.6084/m9.figshare.22285279.v2>.

422

423 **Data availability:** All LGM data can be retrieved from <https://esgf-node.llnl.gov/projects/cmip6/>, all  
424 modern data can be retrieved from references provided. The P Model documentation is available at  
425 <https://pyrealm.readthedocs.io/en/latest/> and the BIOME4 documentation is available at  
426 <https://pmip2.lsce.ipsl.fr/synth/biome4.shtml> and <https://github.com/jedokaplan/BIOME4>.

427

428 **Author contributions.** Experiments conception, strategy and interpretation were developed by O H, ICP and SPH  
429 jointly. OH performed the data processing and analysis, and produced the graphics and Tables. OH wrote the  
430 original draft; SPH and ICP contributed to the final draft.

431

432 **Competing interests.** The contact author has declared that neither themselves nor any other authors have a  
433 conflict of interest.

434

435 **Acknowledgements and financial support.** OH acknowledges support from the NERC Centre for Doctoral  
436 Training in Quantitative and Modelling skills in Ecology and Evolution (Grant No. NE/S007415/1) and from the  
437 Leverhulme Trust through the Leverhulme Centre for Wildfires, Environment and Society (Grant No. RC-2018-  
438 023). Special thanks to David Orme for this help with setting up BIOME4. ICP acknowledges support from the  
439 European Research Council (787203 REALM) under the European Union’s Horizon 2020 research programme.  
440 SPH is supported by the European Research Council (694481 GC2.0) under the same programme. This work is a  
441 contribution to the LEMONTREE (Land Ecosystem Models based On New Theory, obseRvations and  
442 ExperimEnts) project, funded through the generosity of Eric and Wendy Schmidt by recommendation of the  
443 Schmidt Futures program.

#### 444 **References**

445 Abatzoglou, J. T., Williams, A. P., and Barbero, R.: Global emergence of anthropogenic climate change  
446 in fire weather indices, *Geophysical Research Letters*, 46(1), 326–336,  
447 <https://doi.org/10.1029/2018GL080959>, 2019.

448 Albani, S., Balkanski, Y., Mahowald, N., Winckler, G., Maggi, V., and Delmonte, B.: Aerosol-climate  
449 interactions during the Last Glacial Maximum, *Current Climate Change Reports*,4(2), 99–114,  
450 <https://doi.org/10.1007/s40641-018-0100-7>, 2018.

451 Andela, N., Morton, D. C., Giglio, L., Paugam, R., Chen, Y., Hantson, S., Van Der Werf, G. R and  
452 Randerson, J. T.: The Global Fire Atlas of individual fire size, duration, speed and direction, *Earth  
453 System Science Data*, 11(2), 529–552, <https://doi.org/10.5194/essd-11-529-2019>, 2019.

454 Archibald, S., Lehmann, C. E. R., Gómez-Dans, J. L., and Bradstock, R. A.: Defining pyromes and  
455 global syndromes of fire regimes, *Proceedings of the National Academy of Sciences*, 110(16), 6442–  
456 6447, <https://doi.org/10.1073/pnas.1211466110>, 2013.

457 Balch, J.K., Abatzoglou, J.T., Joseph, M.B., Koontz, M.J., Mahood, A.L., McGlinchy, J., Cattau, M.E.  
458 and Williams, A.P.: Warming weakens the night-time barrier to global fire, *Nature*, 602(7897), pp.442-  
459 448, <https://doi.org/10.1038/s41586-021-04325-1>, 2022.

460 Bistinas, I., Harrison, S.P., Prentice, I.C. and Pereira, J.M.C.: Causal relationships versus emergent  
461 patterns in the global controls of fire frequency, *Biogeosciences*, 11(18),pp.5087-5101,  
462 <https://doi.org/10.5194/bg-11-5087-2014>, 2014.

463 Betts, R. A., Golding, N., Gonzalez, P., Gornall, J., Kahana, R., Kay, G., Mitchell, L., and Wiltshire,  
464 A.: Climate and land use change impacts on global terrestrial ecosystems and river flows in the  
465 HadGEM2-ES Earth system model using the representative concentration pathways, *Biogeosciences*,  
466 12(5), 1317–1338, <https://doi.org/10.5194/bg-12-1317-2015>, 2015.

467 Black, M. P., Mooney, S. D. and Haberle, S. G.: The fire, human and climate nexus in the Sydney Basin,  
468 eastern Australia, *The Holocene*, 17(4), <https://doi.org/10.1177/0959683607077024>, 469-480, 2007.

469 Blinkhorn, J., Timbrell, L., Grove, M., and Scerri, E. M. L. (2022). Evaluating refugia in recent human  
470 evolution in Africa, *Philosophical Transactions of the Royal Society B*, 377(1849),20200485,  
471 <https://doi.org/10.1098/rstb.2020.0485>, 2022.

472 Bond, W. J., Midgley, G. F., and Woodward, F. I.: The importance of low atmospheric CO<sub>2</sub> and fire in  
473 promoting the spread of grasslands and savannas, *Global Change Biology*, 9(7), 973–98,  
474 <https://doi.org/10.1046/j.1365-2486.2003.00577.x>, 2003.

475 Bond, W. J., and Midgley, G. F.: Carbon dioxide and the uneasy interactions of trees and savannah  
476 grasses, *Philosophical Transactions of the Royal Society B: Biological Sciences*, 367(1588), 601–612,  
477 <https://doi.org/10.1098/rstb.2011.0182>, 2012.

478 Bowman, D. M. J. S.: The impact of Aboriginal landscape burning on the Australian biota, *The New*  
479 *Phytologist*, 140(3), 385–410, <https://doi.org/10.1046/j.1469-8137.1998.00289.x>, 1998.

480 Bowman, D. M. J. S., Kolden, C. A., Abatzoglou, J. T., Johnston, F. H., van der Werf, G. R. and  
481 Flannigan, M.: Vegetation fires in the Anthropocene, *Nature Reviews Earth and Environment*, 1(10),  
482 500–515, <https://doi.org/10.1038/s43017-020-0085-3>, 2020.

483 Bradstock, R. A.: A biogeographic model of fire regimes in Australia: current and future implications,  
484 *Global Ecology and Biogeography*, 19(2), 145–158, [https://doi.org/10.1111/j.1466-](https://doi.org/10.1111/j.1466-8238.2009.00512.x)  
485 [8238.2009.00512.x](https://doi.org/10.1111/j.1466-8238.2009.00512.x), 2010.

486 Bragg, F. J., Prentice, I. C., Harrison, S. P., Eglinton, G., Foster, P. N., Rommerskirchen, F., and  
487 Rullkötter, J.: Stable isotope and modelling evidence for CO<sub>2</sub> as a driver of glacial–interglacial  
488 vegetation shifts in southern Africa, *Biogeosciences*, 10(3), 2001–2010, [https://doi.org/10.5194/bg-10-](https://doi.org/10.5194/bg-10-2001-2013)  
489 [2001-2013](https://doi.org/10.5194/bg-10-2001-2013), 2013.

490 Buitenwerf, R., Bond, W. J., Stevens, N., and Trollope, W.S.W.: Increased tree densities in South  
491 African savannas:> 50 years of data suggests CO<sub>2</sub> as a driver, *Global Change Biology*, 18(2), 675–684,  
492 <https://doi.org/10.1111/j.1365-2486.2011.02561.x>, 2012.

493 Clarke, H., Nolan, R. H., de Dios, V. R., Bradstock, R., Griebel, A., Khanal, S., and Boer, M. M.: Forest  
494 fire threatens global carbon sinks and population centres under rising atmospheric water demand,  
495 *Nature Communications*, 13(1), 7161. <https://doi.org/10.1038/s41467-022-34966-3>, 2022.

496 Constantine IV, M., Williams, A. N., Francke, A., Cadd, H., Forbes, M., Cohen, T. J., Zhu, X. and  
497 Mooney, S. D.: Exploration of the burning question: a long history of fire in eastern Australia with and  
498 without people, *Fire*, 6(4), 152, <https://doi.org/10.3390/fire6040152>, 2023.

499 Cucchi, M., Weedon, G. P., Amici, A., Bellouin, N., Lange, S., Müller Schmied, H., Hersbach, H., and  
500 Buontempo, C.: WFDE5: bias-adjusted ERA5 reanalysis data for impact studies, *Earth System Science*  
501 *Data*, 12(3), 2097–2120, <https://doi.org/10.5194/essd-12-2097-2020>, 2020.

502 Daniau, A.-L., Bartlein, P.J., Harrison, S.P., Prentice, I.C., Brewer, S., Friedlingstein, P., Harrison-  
503 Prentice, T.I., Inoue, J., Marlon, J.R., Mooney, S., Power, M.J., Stevenson, J., Tinner, W., Andrič, M.,  
504 Atanassova, J., Behling, H., Black, M., Blarquez, O., Brown, K. J., Carcaillet, C., Colhoun, E.,  
505 Colombaroli, D., Davis, B.A.S., D’Costa, D., Dodson, J., Dupont, L., Eshetu, Z., Gavin, D.G., Genries,



506 A., Gebru, T., Haberle, S., Hallett, D. J., Horn, S., Hope, G., Katamura, F., Kennedy, L., Kershaw, P.,  
507 Krivonogov, S., Long, C., Magri, D., Marinova, E., McKenzie, G.M., Moreno, P.I., Moss, P., Neumann,  
508 F.H., Norström, E., Paitre, C., Rius, D., Roberts, N., Robinson, G., Sasaki, N., Scott, L., Takahara, H.,  
509 Terwilliger, V., Thevenon, F., Turner, R.B., Valsecchi, V.G., Vannièrè, B., Walsh, M., Williams, N.,  
510 and Zhang, Y.: Predictability of biomass burning in response to climate changes, *Global*  
511 *Biogeochemical Cycles*, 26(4), <https://doi.org/10.1029/2011GB004249>, 2012.

512 De Dios, V.R., Hedò, J., Camprubí, À.C., Thapa, P., Del Castillo, E.M., de Aragón, J.M., Bonet, J.A.,  
513 Balaguer-Romano, R., Díaz-Sierra, R., Yebra, M. and Boer, M.M.: Climate change induced declines  
514 in fuel moisture may turn currently fire-free Pyrenean mountain forests into fire-prone ecosystems,  
515 *Science of The Total Environment*, 797, p.149104, <https://doi.org/10.1016/j.scitotenv.2021.149104>,  
516 2021.

517 De Faria, B.L., Brando, P.M., Macedo, M.N., Panday, P.K., Soares-Filho, B.S. and Coe, M.T.: Current  
518 and future patterns of fire-induced forest degradation in Amazonia, *Environmental Research Letters*,  
519 12(9), p.095005, <https://doi.org/10.1088/1748-9326/aa69ce>, 2017.

520 Dial, R. J., Maher, C. T., Hewitt, R. E., and Sullivan, P. F.: Sufficient conditions for rapid range  
521 expansion of a boreal conifer, *Nature*, 608(7923), 546–551. [https://doi.org/10.1038/s41586-022-05093-](https://doi.org/10.1038/s41586-022-05093-2)  
522 2, 2022.

523 Diffenbaugh, N. S., Konings, A. G., and Field, C. B.: Atmospheric variability contributes to increasing  
524 wildfire weather but not as much as global warming, *Proceedings of the National Academy of Sciences*,  
525 118(46), e2117876118. <https://doi.org/10.1073/pnas.2117876118>, 2021.

526 Donohue, R. J., Roderick, M. L., McVicar, T. R., and Farquhar, G. D.: Impact of CO<sub>2</sub> fertilization on  
527 maximum foliage cover across the globe's warm, arid environments, *Geophys. Res. Lett.*, 40, 3031–  
528 3035. <https://doi.org/10.1002/grl.50563>, 2013.

529 Duane, A., Castellnou, M. and Brotons, L.: Towards a comprehensive look at global drivers of novel  
530 extreme wildfire events, *Climatic Change*, 165(3-4), p.43, [https://doi.org/10.1007/s10584-021-03066-](https://doi.org/10.1007/s10584-021-03066-4)  
531 4 , 2021.

532 Duffin, K. I.: The representation of rainfall and fire intensity in fossil pollen and charcoal records from  
533 a South African savanna, *Review of Palaeobotany and Palynology*, 151(1–2), 59–71,  
534 <https://doi.org/10.1016/j.revpalbo.2008.02.004>, 2008.

535 Flannigan, M., Cantin, A. S., De Groot, W. J., Wotton, M., Newbery, A., and Gowman, L. M.: Global  
536 wildland fire season severity in the 21st century, *Forest Ecology and Management*, 294, 54–61,  
537 <https://doi.org/10.1016/j.foreco.2012.10.022>, 2013.

538 Fuller, D. Q., Denham, T., Arroyo-Kalin, M., Lucas, L., Stevens, C. J., Qin, L., Allaby, R. G., and  
539 Purugganan, M. D.: Convergent evolution and parallelism in plant domestication revealed by an  
540 expanding archaeological record, *Proceedings of the National Academy of Sciences*, 111(17), 6147–  
541 6152, <https://doi.org/10.1073/pnas.1308937110>, 2014.

542 Gautney, J. R., and Holliday, T. W.: New estimations of habitable land area and human population size  
543 at the Last Glacial Maximum, *Journal of Archaeological Science*, 58, 103–112,  
544 <https://doi.org/10.1016/j.jas.2015.03.028>, 2015.

545 Gonsamo, A., Ciais, P., Miralles, D. G., Sitch, S., Dorigo, W., Lombardozzi, D., Friedlingstein, P.,  
546 Nabel, J. E. M. S., Goll, D. S., O’Sullivan, M. Arneeth, A., Anthoni, P., Jain, A.K., Wiltshire A., Peylin  
547 P., Cescatti A.: Greening drylands despite warming consistent with carbon dioxide fertilization effect,  
548 *Global Change Biology*, 27(14), 3336–3349, <https://doi.org/10.1111/gcb.15658>, 2021.

549 Gott, B: Aboriginal fire management in south-eastern Australia: aims and frequency, *Journal of*  
550 *Biogeography*, 32(7), 1203–1208, <https://www.jstor.org/stable/3566388>, 2005.

551 Grillakis, M., Voulgarakis, A., Rovithakis, A., Seiradakis, K.D., Koutroulis, A., Field, R.D., Kasoar,  
552 M., Papadopoulos, A. and Lazaridis, M.: Climate drivers of global wildfire burned area, *Environmental*  
553 *Research Letters*, 17(4), p.045021, <https://doi.org/10.1088/1748-9326/ac5fa1>, 2022.

554 Grossiord, C., Buckley, T.N., Cernusak, L.A., Novick, K.A., Poulter, B., Siegwolf, R.T., Sperry, J.S.  
555 and McDowell, N.G.: Plant responses to rising vapor pressure deficit, *New Phytologist*, 226(6),  
556 pp.1550-1566, <https://doi.org/10.1111/nph.16485>, 2020.

557 Haas, O., Prentice, I. C., and Harrison, S. P.: Global environmental controls on wildfire burnt area, size,  
558 and intensity, *Environmental Research Letters*, 17(6), 065004, [https://doi.org/10.1088/1748-](https://doi.org/10.1088/1748-9326/ac6a69)  
559 [9326/ac6a69](https://doi.org/10.1088/1748-9326/ac6a69) , 2022.

560 Haas, O: Scripts and input files. figshare. Dataset. <https://doi.org/10.6084/m9.figshare.19071044.v1>,  
561 2023.

562 Haas, O: Data for: The response of wildfire regimes to Last Glacial Maximum carbon dioxide and  
563 climate. figshare. Dataset. <https://doi.org/10.6084/m9.figshare.22285303.v2>, 2023.

564 Haas, O: R scripts to run models for: The response of wildfire regimes to Last Glacial Maximum carbon  
565 dioxide and climate. figshare. Software. <https://doi.org/10.6084/m9.figshare.22285279.v2>, 2023.

566 Hantson, S., Kelley, D. I., Arneeth, A., Harrison, S. P., Archibald, S., Bachelet, D., Forrest, M., Hickler,  
567 T., Lasslop, G., Li, F., Mangeon, S., Melton, J.R., Nieradzik, L., Rabin, S.S., Prentice, I.C., Sheehan,  
568 T., Sitch, S., Teckentrup, L., Voulgarakis, A., and Yue, C.: Quantitative assessment of fire and  
569 vegetation properties in simulations with fire-enabled vegetation models from the Fire Model  
570 Intercomparison Project, *Geoscientific Model Development*, 13(7), 3299–3318,  
571 <https://doi.org/10.5194/gmd-13-3299-2020>, 2020.

572 Harrison, S. P., and Prentice, C. I.: Climate and CO<sub>2</sub> controls on global vegetation distribution at the  
573 last glacial maximum: analysis based on palaeovegetation data, biome modelling and palaeoclimate  
574 simulations, *Global Change Biology*, 9(7), 983–1004, [https://doi.org/10.1046/j.1365-](https://doi.org/10.1046/j.1365-2486.2003.00640.x)  
575 [2486.2003.00640.x](https://doi.org/10.1046/j.1365-2486.2003.00640.x), 2003.

576 Harrison, S. P., Prentice, I. C., Bloomfield, K. J., Dong, N., Forkel, M., Forrest, M., Ningthoujam, R.  
577 K., Pellegrini, A., Shen, Y., and Baudena, M. Cardoso, A.W., Huss, J.C., Joshi J., Oliveras, I., Pausas,

578 J.G. and Simpson, J.K.: Understanding and modelling wildfire regimes: an ecological perspective,  
579 *Environmental Research Letters*, 16(12), 125008, <https://doi.org/10.1088/1748-9326/ac39be>, 2021.

580 Harrison, S.P., Villegas-Diaz, R., Cruz-Silva, E., Gallagher, D., Kesner, D., Lincoln, P., Shen, Y.,  
581 Sweeney, L., Colombaroli, D., Ali, A., Barhoumi, C., Bergeron, Y., Blyakharchuk, T., Bobek, P.,  
582 Bradshaw, R., Clear, J.L., Czerwiński, S., Daniau, A-L., Dodson, J., Edwards, K.J., Edwards, M.E.,  
583 Feurdean, A., Foster, D., Gajewski, K., Gałka, M., Garneau, M., Giesecke, T., Gil Romera, G.,  
584 Girardin, M.P., Hoefler, D., Huang, K., Inoue, J., Jamrichová, E., Jasiunas, N., Jiang, W., Jiménez-  
585 Moreno, G., Karpińska-Kołodziej, M., Kołodziej, P., Kuosmanen, N., Lamentowicz, M., Lavoie, M., Li,  
586 F., Li, J., Lisitsyna, O., López-Sáez, J.A., Luelmo-Lautenschlaeger, R., Magnan, G., Magyari, E.K.,  
587 Maksims, A., Marcisz, K., Marinova, E., Marlon, J., Mensing, S., Mirosław-Grabowska, J., Oswald,  
588 W., Pérez-Díaz, S., Pérez-Obiol, R., Piilo, S., Poska, A., Qin, X., Remy, C.C., Richard, P.J.H., Salonen,  
589 S., Sasaki, N., Schneider, H., Shotyk, W., Stancikaite, M., Šteinberga, D., Stivrins, N., Takahara, H.,  
590 Tan, Z., Trasune, L., Umbanhowar, C.E., Välranta, M., Vassiljev, J., Xiao, X., Xu, Q., Xu, X., Zawisza,  
591 E., Zhao, Y., Zhou, Z., and Paillard, J.: The Reading Palaeofire database: an expanded global resource  
592 to document changes in fire regimes from sedimentary charcoal records, *Earth System Science Data*  
593 ,14: 1109-1124, <https://doi.org/10.5194/essd-14-1109-2022>, 2022.

594 Humber, M. L., Boschetti, L., Giglio, L., and Justice, C. O.: Spatial and temporal intercomparison of  
595 four global burned area products, *International Journal of Digital Earth*, 12(4), 460–484,  
596 <https://doi.org/10.1080/17538947.2018.1433727>, 2019.

597 Jolly, W. M., Cochrane, M. A., Freeborn, P. H., Holden, Z. A., Brown, T. J., Williamson, G. J., and  
598 Bowman, D.: Climate-induced variations in global wildfire danger from 1979 to 2013, *Nature*  
599 *Communications*, 6(1), 1–11, <https://doi.org/10.1038/ncomms8537>, 2015.

600 Kageyama, M., Harrison S.P., Kapsch, M.L., Lofverstrom, M., Lora J.M., Mikolajewicz U., Sherriff-  
601 Tadano,S., Vadsaria T., Abe-Ouchi A., Bouttes N., Chandan, D., Gregoire L.J., Ivanovic, R.F., Kenji  
602 Izumi, Allegra N. LeGrande, Fanny Lhardy, Gerrit Lohmann, Polina A. Morozova, Rumi Ohgaito, Paul,  
603 Peltier W.R., Poulsen, C.J., Quiquet, A., Roche, D.M., Shi, X., Tierney, J.E., Valdes, P.J., Volodin E.  
604 and Zhu J.: The PMIP4-CMIP6 Last Glacial Maximum experiments: preliminary results and  
605 comparison with the PMIP3-CMIP5 simulations, *Climate of the Past* 17: 1065-1089,  
606 <https://doi.org/10.5194/cp-17-1065-2021>, 2021.

607 Kaplan, J.O., Bigelow, Prentice, I.C., Harrison, S.P., P.J., N.H., Bartlein, Christensen, T.R., Cramer,  
608 W., Matveyeva, N.V., McGuire, A.D., Murray, D.F., Razzhivin, V.Y., Smith, B. and Walker, D.A.,  
609 Anderson, P.M., Andreev, A.A., Brubaker, L.B., Edwards, M.E., and Lozhkin, A.V.: Climate change  
610 and Arctic ecosystems II: Modeling, palaeodata-model comparisons, and future projections, *Journal of*  
611 *Geophysical Research-Atmosphere* 108, No. D19, 8171, <https://doi.org/10.1029/2002JD002559>, 2003.

612

613 Kaplan, J. O., Pfeiffer, M., Kolen, J. C. A., and Davis, B. A. S.: Large scale anthropogenic reduction of  
614 forest cover in Last Glacial Maximum Europe. *PLoS One*, 11(11),  
615 <https://doi.org/10.1371/journal.pone.0166726>, 2016.

616 Kgope, B. S., Bond, W. J., and Midgley, G. F.: Growth responses of African savanna trees implicate  
617 atmospheric [CO<sub>2</sub>] as a driver of past and current changes in savanna tree cover, *Austral Ecology*, 35(4),  
618 451–463, <https://doi.org/10.1111/j.1442-9993.2009.02046.x>, 2010.

619 Knorr, W., Jiang, L., and Arneth, A.: Climate, CO<sub>2</sub> and human population impacts on global wildfire  
620 emissions, *Biogeosciences*, 13(1), 267–282, <https://doi.org/10.5194/bg-13-267-2016>, 2016.

621 Knorr, W., Kaminski, T., Arneth, A. and Weber, U.: Impact of human population density on fire  
622 frequency at the global scale, *Biogeosciences*, 11(4), pp.1085-1102, <https://doi.org/10.5194/bg-11-1085-2014>, 2014.

624 Kraaij, T., Engelbrecht, F., Franklin, J., and Cowling, R. M.: A fiery past: A comparison of glacial and  
625 contemporary fire regimes on the Palaeo-Agulhas Plain, Cape Floristic Region, *Quaternary Science  
626 Reviews*, 235, 106059, <https://doi.org/10.1016/j.quascirev.2019.106059>, 2020.

627 Kuhn-Régnier, A., Voulgarakis, A., Nowack, P., Forkel, M., Prentice, I. C., and Harrison, S. P.: The  
628 importance of antecedent vegetation and drought conditions as global drivers of burnt area,  
629 *Biogeosciences*, 18(12), 3861–3879, <https://doi.org/10.5194/bg-18-3861-2021>, 2021.

630 Kumar, D., Pfeiffer, M., Gaillard, C., Langan, L., and Scheiter, S., Climate change and elevated CO<sub>2</sub>  
631 favor forest over savanna under different future scenarios in South Asia, *Biogeosciences*, 18(9), 2957–  
632 2979, <https://doi.org/10.5194/bg-18-2957-2021>, 2021.

633 Li, F., Levis, S., and Ward, D. S. (2013). Quantifying the role of fire in the Earth system - Part 1:  
634 Improved global fire modeling in the Community Earth System Model (CESM1), *Biogeosciences*,  
635 10(4), 2293–2314. <https://doi.org/10.5194/bg-10-2293-2013>, 2013.

636 Li, W., MacBean, N., Ciais, P., Defourny, P., Lamarche, C., Bontemps, S., Houghton, R. A., and Peng,  
637 S.: Gross and net land cover changes in the main plant functional types derived from the annual ESA  
638 CCI land cover maps (1992–2015), *Earth System Science Data*, 10(1), 219–234,  
639 <https://doi.org/10.5194/essd-10-219-2018>, 2018.

640 Liu, L., Bestel, S., Shi, J., Song, Y., and Chen, X.: Paleolithic human exploitation of plant foods during  
641 the last glacial maximum in North China, *Proceedings of the National Academy of Sciences of the  
642 United States of America*, 110(14), 5380–5385. <https://doi.org/10.1073/pnas.1217864110>, 2013.

643 Lohmann, G., Butzin, M., Eissner, N., Shi, X., and Stepanek, C.: Abrupt climate and weather changes  
644 across time scales, *Paleoceanography and Paleoclimatology*, 35(9),  
645 <https://doi.org/10.1029/2019PA003782>, 2020.

646 Marlon, J.R., Bartlein, P.J., Carcaillet, C., Gavin, D.G., Harrison, S.P., Higuera, P.E., Joos, F., Power,  
647 M.J. and Prentice, I.C.: Climate and human influences on global biomass burning over the past two  
648 millennia, *Nature Geoscience*, 1(10), pp.697-702, <https://doi.org/10.1038/ngeo313>, 2008.

649 Marlon, J.R., Kelly, R., Daniau, A.-L., Vanni re, B., Power, M. J., Bartlein, P., Higuera, P., Blarquez,  
650 O., Brewer, S., Br ucher, T, Feurdean A., Romera G.G., Iglesias V., Maezumi S.Y., Magi, B., Courtney  
651 Mustaphi, C.J., and Zhihai, T.: Reconstructions of biomass burning from sediment-charcoal records to  
652 improve data–model comparisons, *Biogeosciences*, 13(11), 3225–3244, [https://doi.org/10.5194/bg-13-](https://doi.org/10.5194/bg-13-3225-2016)  
653 3225-2016, 2016.

654 Martin Calvo, M., and Prentice, I. C.: Effects of fire and CO<sub>2</sub> on biogeography and primary production  
655 in glacial and modern climates, *New Phytologist*, 208(3), 987–994, <https://doi.org/10.1111/nph.13485>,  
656 2014.

657 Martin Calvo, M., Prentice, I. C., and Harrison, S. P.: Climate versus carbon dioxide controls on  
658 biomass burning: a model analysis of the glacial–interglacial contrast, *Biogeosciences*, 11(21), 6017–  
659 6027, <https://doi.org/10.5194/bg-11-6017-2014>, 2014.

660 Mauritsen, T., Bader, J., Becker, T., Behrens, J., Bittner, M., Brokopf, R., Brovkin, V., Claussen, M.,  
661 Crueger, T., Esch, M., Fast I., Fiedler S., Fl schner D., Gayler V., Giorgetta M., Goll D.S., Haak H.,  
662 Hagemann S., Hedemann C., Hohenegger C., Ilyina, T., Jahns T., Jimen ez-de-la-Cuesta, D., Jungclaus  
663 J., Kleinen T., Kloster S., Kracher D., Kinne S., Kleberg D., Lasslop G., Kornblueh L., Marotzke J.,  
664 Matei D., Meraner K., Mikolajewicz U., Modali K., M obis, B., M uller A.W., Julia E. M. S. Nabel, J.E.  
665 M. S, Nam C.C.W., Notz D., Nyawira S., Paulsen H., Peters K., Pincus R., Pohlmann H., Pongratz J.,  
666 Popp M., J urgen Raddatz T., Rast S., Redler,R., Reick, C.H., Rohrschneider, T., Schemann V.,  
667 Schmidt, H., Schnur R., Schulzweida, U., Six K.D., Stein, L., Stemmler, I., Stevens B., Storch J-S.V,  
668 Tian F., Voigt, A., Vrese, P., Wieners K., Wilkenskjeld, S., Winkler A., Roeckner, E.: Developments  
669 in the MPI-M Earth System Model version 1.2 (MPI-ESM1. 2) and its response to increasing CO<sub>2</sub>,  
670 *Journal of Advances in Modeling Earth Systems*, 11(4), 998–1038,  
671 <https://doi.org/10.1029/2018MS001400>, 2019.

672 Moreno, P. I., Videla, J., Valero-Garc es, B., Alloway, B. v, and Heusser, L. E.: A continuous record of  
673 vegetation, fire-regime and climatic changes in northwestern Patagonia spanning the last 25,000 years,  
674 *Quaternary Science Reviews*, 198, 15–36, <https://doi.org/10.1016/j.quascirev.2018.08.013>, 2018.

675 Pausas, J. G.: Bark thickness and fire regime, *Functional Ecology*, 29(3), 315–327,  
676 <https://doi.org/10.1111/1365-2435.12372>, 2014.

677 Pausas, J. G., and Keeley, J. E.: Wildfires and global change, *Frontiers in Ecology and the Environment*,  
678 19(7), 387–395, <https://doi.org/10.1002/fee.2359>, 2021.

679 Pausas, J. G., and Ribeiro, E.: The global fire–productivity relationship, *Global Ecology and*  
680 *Biogeography*, 22(6), 728–736, <https://doi.org/10.1111/geb.12043>, 2013.

681 Pechony, O., and Shindell, D. T.: Driving forces of global wildfires over the past millennium and the  
682 forthcoming century, *Proceedings of the National Academy of Sciences*, 107(45), 19167-19170,  
683 <https://doi.org/10.1073/pnas.1003669107>, 2010.

684 Peltier, W. R., Argus, D. F., and Drummond, R.: Space geodesy constrains ice age terminal  
685 deglaciation: The global ICE-6G\_C (VM5a) model, *Journal of Geophysical Research: Solid Earth*,  
686 *120*(1), 450–487, <https://doi.org/10.1002/2014JB011176>, 2015.

687 Piao, S., Wang, X., Park, T., Chen, C., Lian, X. U., He, Y., Bjerke, J. W., Chen, A., Ciais, P.,  
688 Tømmervik, H., Nemani R.R. and Myneni R.B.: Characteristics, drivers and feedbacks of global  
689 greening, *Nature Reviews Earth and Environment*, *1*(1), 14–27, [https://doi.org/10.1038/s43017-019-](https://doi.org/10.1038/s43017-019-0001-x)  
690 0001-x, 2020.

691 Portenga, E. W., Rood, D. H., Bishop, P., and Bierman, P. R.: A late Holocene onset of Aboriginal  
692 burning in southeastern Australia, *Geology*, *44*(2), 131–134, <https://doi.org/10.1130/G37257.1>, 2016.

693 Power, M.J., Ortiz, N., Marlon, J., Bartlein, P.J., Harrison, S.P., Mayle, F., Ballouche, A., Bradshaw,  
694 R., Carcaillet, C., Cordova, C., Mooney, S., Moreno, P., Prentice, I.C., Thonicke, K., Tinner, W.,  
695 Whitlock, C., Zhang, Y., Zhao, Y., Anderson, R.S., Beer, R., Behling, H., Briles, C., Brown, K., Brunelle  
696 A., Bush, M., Clark, J., Colombaroli, D., Chu, C. Q., Daniels, M., Dodson, J., Edwards, M.E., Fisinger,  
697 W., Gavin, D.G., Gobet, E., Hallett, D.J., Higuera, P., Horn, S., Inoue, J., Kaltenrieder, P., Kennedy,  
698 L., Kong, Z.C., Long, C., Lynch, J., Lynch, B., McGlone, M., Meeks, S., Meyer, G., Minckley, T.,  
699 Mohr, J., Noti, R., Pierce, J., Richard, P., Shuman, B.J., Takahara, H., Toney, J., Turney, C.,  
700 Umbanhower, C., Vandergoes, M., Vanniere, B., Vescovi, E., Walsh, M., Wang, X., Williams, N.,  
701 Wilmshurst, J., and Zhang, J.H.: Changes in fire regimes since the Last Glacial Maximum: an  
702 assessment based on a global synthesis and analysis of charcoal data, *Climate Dynamics*, *30*(7), 887–  
703 907, <https://doi.org/10.1007/s00382-007-0334-x>, 2008.

704 Rodrigues, M., Costafreda-Aumedes, S., Comas, C., and Vega-García, C.: Spatial stratification of  
705 wildfire drivers towards enhanced definition of large-fire regime zoning and fire seasons, *Science of the*  
706 *Total Environment*, *689*, 634–644, <https://doi.org/10.1016/j.scitotenv.2019.06.467>, 2019.

707 Rogers, B. M., Balch, J. K., Goetz, S. J., Lehmann, C. E. R., and Turetsky, M.: Focus on changing fire  
708 regimes: interactions with climate, ecosystems, and society, *Environmental Research Letters*, *15*(3),  
709 030201, <https://doi.org/10.1088/1748-9326/ab6d3a>, 2020.

710 Rowe, C., Wurster, C. M., Zwart, C., Brand, M., Hutley, L. B., Levchenko, V., and Bird, M. I.:  
711 Vegetation over the last glacial maximum at Girraween Lagoon, monsoonal northern Australia,  
712 *Quaternary Research*, *102*, 39–52, <https://doi.org/10.1017/qua.2020.50>, 2021.

713 Ruan, Y., Mohtadi, M., Dupont, L. M., Hebbeln, D., van der Kaars, S., Hopmans, E. C., Schouten, S.,  
714 Hyer, E. J., and Schefuß, E.: Interaction of fire, vegetation, and climate in tropical ecosystems: A  
715 multiproxy study over the past 22,000 years, *Global Biogeochemical Cycles*, *34*(11),  
716 <https://doi.org/10.1029/2020GB006677>, 2020.

717 Rubino, M., D’Onofrio, A., Seki, O., and Bendle, J. A.: Ice-core records of biomass burning, *The*  
718 *Anthropocene Review*, *3*(2), 140–162, <https://doi.org/10.1177/205301961560511>, 2015.

719

720 Scheiter, S., Kumar, D., Corlett, R. T., Gaillard, C., Langan, L., Lapuz, R. S., Martens, C., Pfeiffer, M.,  
721 and Tomlinson, K. W.: Climate change promotes transitions to tall evergreen vegetation in tropical  
722 Asia, *Global Change Biology*, 26(9), 5106–5124, <https://doi.org/10.1111/gcb.15217>, 2020.

723 Schertzer, E., Staver, A. C., and Levin, S. A.: Implications of the spatial dynamics of fire spread for the  
724 bistability of savanna and forest. *Journal of Mathematical Biology*, 70(1), 329–341.  
725 <https://doi.org/10.1007/s00285-014-0757-z>, 2015.

726 Sedano, F., and Randerson, J. T.: Multi-scale influence of vapor pressure deficit on fire ignition and  
727 spread in boreal forest ecosystems, *Biogeosciences*, 11(14), 3739–3755, [https://doi.org/10.5194/bg-11-](https://doi.org/10.5194/bg-11-3739-2014)  
728 3739-2014, 2014.

729 Sidorenko, D., Rackow, T., Jung, T., Semmler, T., Barbi, D., Danilov, S., Dethloff, K., Dorn, W., Fieg,  
730 K., Gößling, H. F., Handorf, D., Harig S., Hiller W., Juricke S., Losch M., Schröter J., Sein D.V. and  
731 Wang Q.: Towards multi-resolution global climate modeling with ECHAM6–FESOM. Part I: model  
732 formulation and mean climate, *Climate Dynamics*, 44, 757–780, [https://doi.org/10.1007/s00382-014-](https://doi.org/10.1007/s00382-014-2290-6)  
733 2290-6, 2015.

734 Snitker, G.: Identifying natural and anthropogenic drivers of prehistoric fire regimes through simulated  
735 charcoal records, *Journal of Archaeological Science*, 95, 1–15,  
736 <https://doi.org/10.1016/j.jas.2018.04.009>, 2018.

737 Song, M., Dodson, J., Lu, F., Shi, G., and Yan, H.: A continuous paleorecord of vegetation and  
738 environmental change from Erxianyan Wetland over the past 60,000 years in central China,  
739 *Palaeogeography, Palaeoclimatology, Palaeoecology*, 111399,  
740 <https://doi.org/10.1016/j.palaeo.2023.111399>, 2023.

741 Song, Y., Jiao, W., Wang, J., and Wang, L.: Increased global vegetation productivity despite rising  
742 atmospheric dryness over the last two decades, *Earth's Future*, 10(7),  
743 <https://doi.org/10.1029/2021EF002634>, 2022.

744 Stocker, B. D., Wang, H., Smith, N. G., Harrison, S. P., Keenan, T. F., Sandoval, D., Davis, T., and  
745 Prentice, I. C.: P-model v1. 0: an optimality-based light use efficiency model for simulating ecosystem  
746 gross primary production, *Geoscientific Model Development*, 13(3), 1545–1581,  
747 <https://doi.org/10.5194/gmd-13-1545-2020>, 2020.

748 Tallavaara, M., Luoto, M., Korhonen, N., Järvinen, H. and Seppä, H.: Human population dynamics in  
749 Europe over the Last Glacial Maximum, *Proceedings of the National Academy of Sciences*, 112(27),  
750 pp.8232-8237, <https://doi.org/10.1073/pnas.1503784112>, 2015.

751 Tierney, J. E., Zhu, J., King, J., Malevich, S. B., Hakim, G. J., and Poulsen, C. J.: Glacial cooling and  
752 climate sensitivity revisited, *Nature*, 584(7822), 569–573, <https://doi.org/10.1038/s41586-020-2617-x>,  
753 2020.

754 Van der Sleen, P., Groenendijk, P., Vlam, M., Anten, N. P. R., Boom, A., Bongers, F., Pons, T. L.,  
755 Terburg, G., and Zuidema, P. A.: No growth stimulation of tropical trees by 150 years of CO<sub>2</sub>

756 fertilization but water-use efficiency increased, *Nature Geoscience*, 8(1), 24–28.  
757 <https://doi.org/10.1038/ngeo2313>, 2015.

758 Wang, H., Prentice, I. C., Keenan, T. F., Davis, T. W., Wright, I. J., Cornwell, W. K., Evans, B. J., and  
759 Peng, C.: Towards a universal model for carbon dioxide uptake by plants, *Nature Plants*, 3(9), 734–  
760 741, <https://doi.org/10.1038/s41477-017-0006-8>, 2017.

761 Williams, A. N., Ulm, S., Cook, A. R., Langley, M. C., and Collard, M.: Human refugia in Australia  
762 during the Last Glacial Maximum and terminal Pleistocene: A geospatial analysis of the 25–12 ka  
763 Australian archaeological record, *Journal of Archaeological Science*, 40(12), 4612–4625,  
764 <https://doi.org/10.1016/j.jas.2013.06.015>, 2013.

765 Williams A.P., Allen C.D., Macalady A.K., Griffin D., Woodhouse C.A., Meko D.M., Swetnam T.W.,  
766 Rauscher S.A., Seager R., Grissino-Mayer H.D., Dean J.S., Cook E.R., Gangodagamage C., Cai M.  
767 and McDowell N.G.: Temperature as a potent driver of regional forest drought stress and tree mortality,  
768 *Nature Climate Change* 3: 292–297, <https://doi.org/10.1038/nclimate1693>, 2013.